SCALING ANALYSIS OF A MEMS-BASED RESONANT MICRO HEAT ENGINE

H. Bardaweel[1], B.S. Preetham[1], M. A. Brubaker[1], R. Richards[1], M. Anderson[2], C. Richards[1*]
[1] School of Mechanical and Materials Engineering, Washington State University, Pullman, WA, USA
[2] Dept. of Mechanical Engineering, University of Idaho
*Presenting Author: heatran@wsu.edu

Abstract: In this work we investigate issues related to scaling of a MEMS-based resonant heat engine. We use both experiment and model. A scaling model of the resonant micro heat engine is developed and experiments are performed. The results show that the performance of the engine is mainly determined by three major factors: geometry of the engine, speed of operation, and the thermal physical properties of the engine components. The results suggest that larger engine volumes, working fluids with higher latent heats of evaporation, slower engine speeds, and more compliant structures are desirable.

Keywords: MEMS-based resonant heat engine, lumped parameter model

INTRODUCTION

Much research effort has been devoted to the development of micro-scale heat engines based on existing macro-scale versions [1-5]. However, scaling macro-scale designs down to the micro-scale presents many difficulties. The design of the MEMS-based resonant micro heat engine, presented in this work, avoids many of the challenging issues related to scaling from macro-scale to micro-scale. First, the resonant micro heat engine is an external combustion engine; thereby issues related to micro-scale combustion quenching are eliminated. Second, the design of the engine is based on stacking two dimensional structures and thus eliminates the fabrication challenge associated with complex three dimensional features. Third, flexing components rather than rotating or reciprocating parts are used. The use of flexing components eliminates high stresses on some parts of the engine. Also, the micro heat engine, presented in this article, is a resonant-type engine. In previous work the resonant frequency of the engine was determined to be in the order of 100 Hz [6,7]. The low operational frequency of the resonant engine mitigates losses due to friction and viscous damping.

A consequence of using flexing, resonating, components in the micro heat engine is that coupling between dynamics, thermodynamics and heat transfer within the engine becomes very crucial. In this work we perform scaling analysis on this MEMS-based resonant micro heat engine and develop a scaling model.

APPROACH

Experiment

The engine, shown in Fig. 1, consists of a cavity filled with a two-phase fluid bounded by top and bottom membranes. The flexible top membrane acts as an expander, while, the rigid bottom membrane as an evaporator. A capillary wick fabricated on the bottom membrane controls the layer of liquid-phase working fluid on the evaporator. Details on the fabrication, assembly, and operation are provided in [6-8].

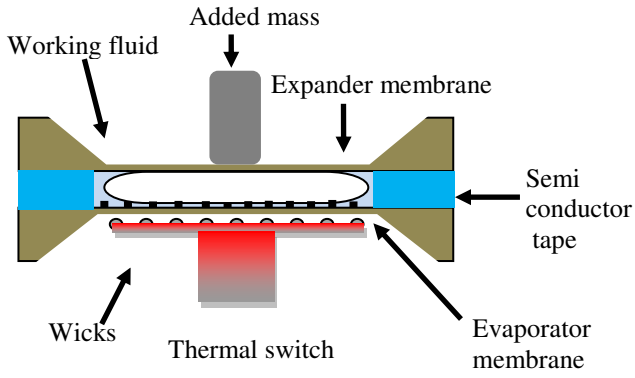

Fig. 1: Schematic of the micro heat engine.

A function generator was used for delivering a unipolar periodic square voltage wave $V_h(t)$ to a resistance heater to enabled precise control over the magnitude and duration of the heat addition process for comparison to the model. This level of control was required to effectively resolve the spectral behavior of the micro heat engine using the transfer function approach.

Each time the voltage is applied, through the resistance heater, electrical power is dissipated as heat and transferred into the rigid evaporator membrane. The heat transferred into the cavity evaporates liquid working fluid, causing a pressure increase inside the thereby deflecting expander membrane upward, as a result producing mechanical work. Heat rejection from the cavity results in condensation of the vapor and causes the expander membrane to flex inward. Thus, the expander membrane undergoes periodic motion due to heat addition and heat rejection. A laser vibrometer is used to measure the periodic motion x(t) of the expander. The motion of the expander x(t) and the heater voltage $V_h(t)$ are sampled with a digital oscilloscope and stored for later analysis.

A linear-systems transfer function approach is then used to interpret the experimental data. The input to the system is taken to be the heat rate input into the engine, q(t), computed from the measured heater

voltage using $q(t)=V_h^2(t)/R_h$, where R_h is the resistance across the heater. The output from the system is taken to be the velocity of the expander membrane $\boldsymbol{u(t)} = \boldsymbol{\dot{x}(t)}$. The experimentally determined periodic heat input is represented by the Fourier series

$$q(t)=Q_o+\sum_k Q_k \cos(2\pi f_k t+\theta_k) \quad (1)$$

where f_k are the harmonic frequencies $f_k = k/T_P$, T_P is the period of the engine cycle operation, Q_k and θ_k are the amplitudes and phases, respectively. The k amplitudes Q_k and phases θ_k are extracted from the heat input q(t) using an FFT algorithm. The number of k components is determined by the number of sampled points in a measured waveform. Likewise the experimentally determined periodic velocity of the expander membrane is represented by the Fourier series

$$u(t)=U_0+\sum_k U_k \cos(2\pi f_k t+\gamma_k) \quad (2)$$

As before, amplitudes, U_k, and phases, γ_k, are extracted from the velocity of the expander membrane, u(t), using an FFT algorithm. Interpretation of the performance of the engine is then reduced to predicting the system transfer function $\Gamma(f_K)$ between the coefficients Q_k, and U_k at each of the k frequencies f_k, i.e.

$$\Gamma(f_k)=\frac{U_k}{Q_k} \quad (3)$$

Model

In previous work a lumped parameter model of the micro heat engine was developed and validated against measured data [6,7]. The lumped parameter model of the engine is obtained by applying conservation laws to the vapor bubble and liquid film above the evaporator and Newton's laws for the motion of the expander and evaporator membranes. Fig. 2 shows the model schematic of the micro heat engine.

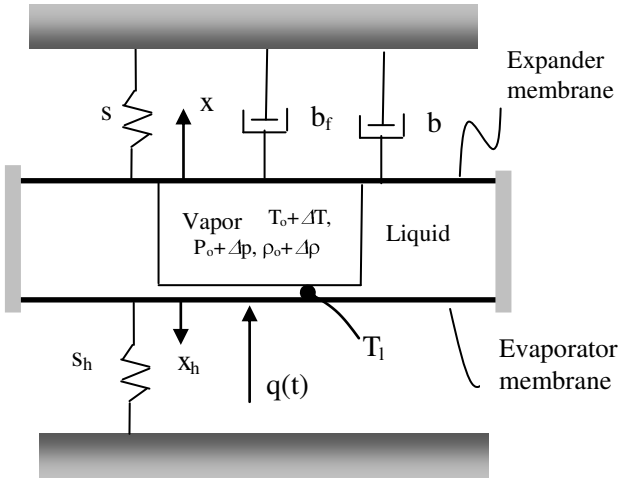

Fig. 2: Model schematic of the micro heat engine.

Details on model development and validation are provided in [6]. To obtain a nondimensional form of the model we define

$$\Delta V^* = \frac{\Delta V}{V_o},\ \Delta P^* = \frac{\Delta P}{P_o},\ \Delta T_l^* = \frac{\Delta T_l}{T_o},$$
$$q^* = \frac{q}{\omega \rho_o h_{fg} V_o},\ t^* = \omega t, \quad (4)$$

where ΔV is the volume change of the vapor bubble caused by motion of the upper membrane; Δp, ΔT, and ΔT_l are the departures of vapor pressure, temperature, and liquid temperature from their ambient values. The frequency ω is a reference mechanical frequency given by $\omega = \sqrt{s/(m+\bar{m})}$. Neglecting evaporator membrane flexibility and parasitic heat losses from the vapor bubble, a nondimensional form of the model engine is given by

$$\begin{bmatrix} 1 & 0 & 0 & 0 \\ \frac{1}{Q} & 1 & 0 & 0 \\ 1 & 0 & 1 & 0 \\ 0 & 0 & 0 & C \end{bmatrix} \begin{Bmatrix} \dot{\Delta V}^* \\ \ddot{\Delta V}^* \\ \dot{\Delta p}^* \\ \dot{\Delta T_l}^* \end{Bmatrix} =$$

$$\begin{bmatrix} 0 & 1 & 0 & 0 \\ -1 & 0 & F\Phi & 0 \\ 0 & 0 & -N\Phi\frac{\gamma+1}{2\gamma} & N\Phi(BT_o) \\ 0 & 0 & N\Phi\frac{\gamma+1}{2\gamma} & -\bar{U}+(BT_o)N\Phi \end{bmatrix} \begin{Bmatrix} \dot{\Delta V}^* \\ \Delta V^* \\ \dot{\Delta p}^* \\ \Delta T_l^* \end{Bmatrix} \quad (5)$$

where

$$Q=\frac{m\omega}{b+b_f},\quad F=\frac{\pi r_o^2 P_o}{m\omega},\quad N=\frac{1}{\rho_o}\sqrt{\frac{M}{2\pi R_u}}\frac{P_o}{\sqrt{T_o}},$$
$$\Phi=\frac{S}{\omega V_o},\quad C=C_T\frac{T_o}{\rho_o h_{fg} V_o},\quad \bar{U}=\frac{U}{\omega}\frac{T_o}{\rho_o h_{fg} V_o}. \quad (6)$$

The scaling model described by (5) reveals the nondimensional numbers Q, C, $\bar{U}$ and products $F\Phi$ and $N\Phi$. The nondimensional numbers C and $\bar{U}$ account for thermal inertia and parasitic conductive heat losses, respectively. The nondimensional number, Q is the quality factor describing energy losses due to damping and viscous effects. The quantities F, N, and Φ account for mechanical properties associated with engine flexing, thermal properties of the working fluid, and time-geometry properties of the engine.

RESULTS AND DISCUSSION

To investigate the scaling issues related to the micro heat engine, a set of experiments was performed in which the expander membrane material and thickness, and the thickness of engine cavity were

varied. The side lengths of the expander and evaporator membranes were fixed at 10 mm and 8 mm, respectively. The engine cavity was filled with a two phase-mixture of 3M™ PF5060DL working fluid. The size of the vapor bubble was 9 mm. The wicks were 5μm thick, 10μm high, and spaced 90μm apart. A mass was placed on top of the expander membrane. The engine was operated by applying periodic unipolar heat pulses with fundamental frequencies of f_o =0.1, 1 and 10.0 Hz with durations of T = 100, 10 and 1.0 ms, respectively. The input energy, per cycle, delivered to the engine was E=9 mJ. Table 1 lists the specifications of the micro heat engines used in this work. In Table 1, engine I is used as the nominal case for engine performance comparison.

Table 1: Engine Specifications

Engine Specification	Engine I	Engine II	Engine III	Engine IV
Expander Material	Silicon	Silicon	Silicon Nitride	PDMS
Expander thickness (μm)	2.00	2.00	0.30	0.95
Cavity thickness (μm)	450	75	150	450
Mass added(g)	4.00	4.00	4.00	0.56

Fig. 3 shows, both, measured and modeled transfer functions of the tested engines. In the model, the geometrical conditions of the engine, environmental conditions, and working fluid properties are known parameters. Thermal storage C_T, heat loss coefficients U_c and U_B, damping coefficient b_f, and the total effective mass $m+\overline{m}$ are unknown floating parameters in the model. Since no energy convertor was attached to the engines, the useful damping coefficient was set equal to zero, i.e. b=0. The floating parameters are determined by comparing the modeled velocity transfer function to the measured one. Details on obtaining the unknown floating parameters and model fitting are provided in [7,8]. Fig. 4, reveals the importance of time-geometry factor, Φ and nondimensional thermal inertia, C in determining the performance of the engine. In Fig. 4, the performance of the engines is compared based on the maximum velocity amplitudes, V_{max} appearing in the transfer functions of the engines. The nominal velocity, V_I is defined as the maximum velocity amplitude of engine I in Table 1. The nominal values of the time-geometry factor, Φ_I and the nondimensional thermal inertial, C_I are computed for engine I, using (6).

For engine I, the nominal case, the ratios of the time-geometry factor and the nondimensional thermal inertia are Φ/Φ_I =1 and C/C_I =1, respectively.

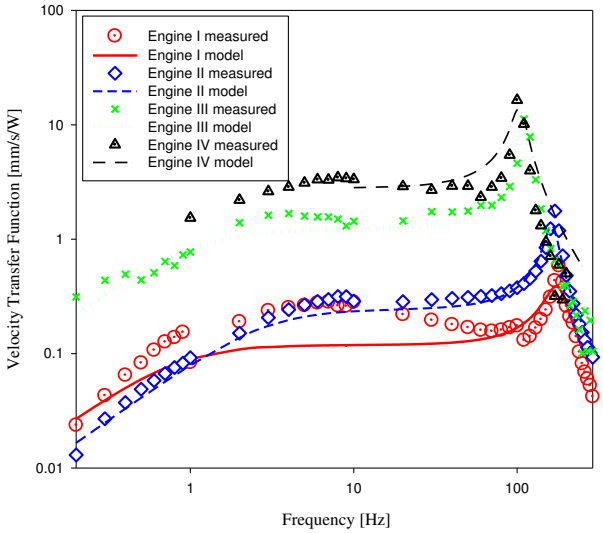

Fig.3: Velocity transfer functions of the tested engines.

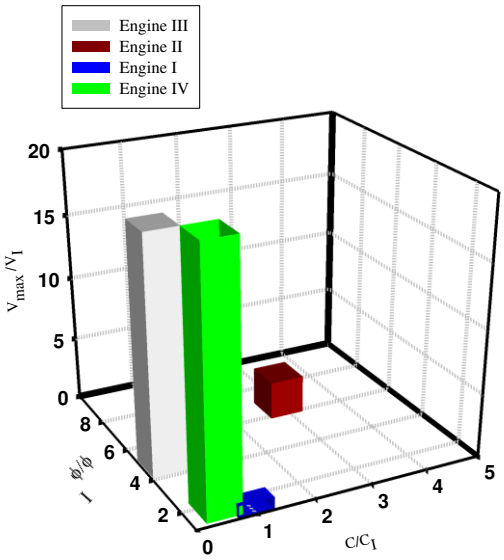

Fig.4: Performance comparison of the micro heat engines.

However, for engine III, the time-geometry factor is raised by a factor of 4.7, i.e. Φ/Φ_I=4.7 and the nondimensional thermal inertia is reduced to one third, i.e. C/C_I=0.335. The velocity amplitude of the engine was increased by a factor of 18.33, i.e. V_{max}/V_I =18.33 from engine I to engine III. An engine with higher time-geometry factor Φ and lower nondimensional thermal inertia C is desirable.

In this work, it is hypothesized that the nondimensional thermal inertia C, the time-geometry factor Φ, and the working fluid evaporation property N are the parameters that dominate the performance of the resonant micro heat engine. The composition of these quantities implies that the performance of the resonant micro heat engine is defined by three factors: geometry of the engine, speed of operation, and thermal physical properties of the engine components.

In the nondimensional thermal inertia C, the dimensional lumped thermal inertia parameter C_T is scaled against the engine vapor volume V_o, and the latent evaporation property $\rho_o h_{fg}$ of the working fluid N. If the working fluid N is fixed, then the nondimensional thermal inertia C scales against the inverse of engine vapor volume V_o. Consequently, the nondimensional thermal inertia C will decrease for larger engine volume.

The nondimensional thermal inertia C is inversely proportional to the latent evaporation property, $\rho_o h_{fg}$ of the working fluid inside the engine cavity. Thus, the nondimensional thermal inertia C will decrease for working fluids with higher latent evaporation property $\rho_o h_{fg}$. The time-geometry factor Φ is composed of the reference frequency ω, and the ratio of evaporation-area to engine volume, i.e. S/V_o. For a fixed S/V_o the time-geometry factor Φ is inversely proportional to the speed of the operation. As a result, lower operating speed will result in higher time-geometry factor Φ and, thus, better engine performance. Increasing the effective mass of the engine or reducing the stiffness of the expander membrane will reduce the reference frequency, $\omega = \sqrt{s/(m+\overline{m})}$, and thereby increase the time-geometry factor Φ. Reducing the reference frequency of the engine may be achieved by adapting more compliant structures or larger engines. For example, although engine II and engine III, both had the same added mass, i.e. m_{added}= 4g, their resonant frequencies shifted from 170 Hz for engine II to 110 Hz for engine III. This is, presumably, due to reduction in stiffness of the top expander membrane. That is, the 300 nm thick silicon nitride membrane used in engine III is more compliant than the 2 μm thick silicon membrane used in engine II. Interestingly, even though very small amount mass of 0.5g was added to the engine IV, the resonant frequency was lesser than engines II and III, which could be attributed to the low stiffness of fabricated PDMS membranes. The time-geometry factor and the velocity amplitude calculations for engine IV were found to be 1.77 and 28.47 respectively. The high velocity amplitude for engine IV suggests low damping compared to engine I.

Increasing the ratio S/V_o will increase time-geometry factor Φ. However, increasing S/V_o will be unfavorable for heat transfer, and so it is desirable to keep S/V_o constant or even decrease it. It is possible to scale up the engine while keeping the ratio S/V_o constant by increasing the side length of the membrane and by maintaining the thickness of the engine cavity, h.

CONCLUSIONS

In this work, a scaling model of the resonant micro heat engine is presented. Experiments were performed to investigate the scaling model in depth. In experiments the expander membrane material and thickness, and the thickness of engine cavity were varied. Scaling analysis shows that the performance of the engine is determined by three major factors: geometry of the engine, speed of operation, and the thermal physical properties of the engine components. The results suggest that larger engine volumes, working fluids with higher latent heats of evaporation, slower engine speeds, and more compliant expander structures are desirable.

ACKNOWLEDGEMENTS

M. A. Brubaker gratefully acknowledges the support of the National Science Foundation Research for Undergraduates Program under grant EEC-0754370.

REFERENCES

1. Frechette L, Lee C, Arslan S, and Liu Y-C 2003 Design of a Microfabricated Rankine Cycle Steam Turbine for Power Generation Paper No. IMECE2003-42082 (Washington, D.C.)
2. Fu K, Knobloch A J, Marinez F C, Walther D C, Fernandez-Pello C, Pisano A P, and Liepmann D 2001 Design and Fabrication of a Silicon Based MEMS Rotary Engine Paper No. IMECE2001/MEMS-23925 (New York, NY)
3. Isomura K, Murayama M, Teramoto S, Hikichi K, Endo Y, Togo S, and Tanaka S 2006 Experimental Verification of The Feasibility of a 100 W Class Micro-Scale Gas Turbine at an Impeller Diameter of 10mm J. Micromech. Microeng. **16** S254- S261
4. Mehra A, Zhang X, Ayon A A, Waitz I A, Schmidt M A, and Spadaccini C M 2000 A Six-Wafer Combustion System for a Silicon Micro Gas Turbine Engine J. MEMS **9** (4) 517–527.
5. Herrault, F., Crittenden, T., Yorish, S., Birdsell, E., Glezer A, and Allen M G 2008 A Self-Resonant, MEMS-Fabricated, Air-Breathing Engine Solid-State Sensors, Actuators, and Microsystems Workshop, Hilton Head Island, South Carolina.
6. Bardaweel H K, Anderson M J, Richards R F, and Richards C D 2008 Optimization of the Dynamic and Thermal Performance of a Resonant Micro Heat Engine J. Micromech. Microeng. **18** (10) 104014.
7. Bardaweel H, Anderson M, Richards R, and Richards C D 2010 Cyclic Operation of a MEMS-Based Resonant Micro Heat Engine: Experiment and Model J. Appl. Phys., **107**, 104901.
8. Cho H, Weiss L W, Richards C D, Bahr D F, and Richards R F 2007 Power Production by a Dynamic Micro Heat Engine with an Integrated Thermal Switch J. Micromech. Microeng., **17** (9) S217-S223.